IEEE Access
Multidisciplinary ⋮ Rapid Review ⋮ Open Access Journal

Received 15 August 2024, accepted 26 August 2024, date of publication 29 August 2024, date of current version 10 September 2024.

Digital Object Identifier 10.1109/ACCESS.2024.3451664

RESEARCH ARTICLE

Design and Optimization of Broadband Directional Couplers and Power Dividers Using SIW Technology

RAÚL HARO-BÁEZ[1], (Senior Member, IEEE), HENRY CARVAJAL MORA[2], (Senior Member, IEEE), NATHALY OROZCO GARZÓN[2], (Senior Member, IEEE), KATHERINE HERRERA[3], AND DIEGO BENÍTEZ[3], (Senior Member, IEEE)

[1]Grupo de Investigación en Sistemas Inteligentes (WiCOM-Energy), Departamento de Eléctrica y Electrónica, Universidad de las Fuerzas Armadas—ESPE, Sangolquí 171103, Ecuador
[2]Faculty of Engineering and Applied Sciences, Telecommunications Engineering, ETEL Research Group, Universidad de Las Américas (UDLA), Quito 170503, Ecuador
[3]Indra Solutions TI S.L., 28037 Madrid, Spain
[4]Colegio de Ciencias e Ingenierías "El Politécnico," Universidad San Francisco de Quito (USFQ), Quito 170157, Ecuador

Corresponding author: Henry Carvajal Mora (henry.carvajal@udla.edu.ec)

The work of Henry Carvajal Mora and Nathaly Orozco Garzón was supported by Universidad de Las Américas under Project 485XIV.24.

ABSTRACT This paper introduces a streamlined design that includes a broadband directional coupler, a set of three-port union-T power dividers, and several microstrip transitions. These components leverage substrate-integrated waveguide (SIW) technology, operating across multiple frequency bands and offering equal power distribution in all output ports. The directional coupler, dividers, and transitions underwent a comprehensive design, simulation, and optimization process using CST Microwave Studio. A crucial aspect of the SIW design was the meticulous consideration of transitions necessary to achieve optimal matching between the SIW devices and the connected structure (such as microstrip or SMA connectors). This approach ensured a consistent focus on seamless integration. For validation purposes, the devices were manufactured physically using the RF-5880 substrate, which works with frequencies up to 40 GHz. The experimental results were then compared with simulations conducted in CST Microwave Studio, validating the prototypes. The findings confirmed that the design performs as intended, exhibiting expected behavior and showcasing a notable agreement between the simulation and experimental results. Furthermore, the designs were treated as standard rectangular waveguides, functioning within microwave and millimeter wave frequencies ranging from 8 to 40 GHz. The paper not only outlines these designs but also proposes practical dimensions for SIW technology, offering a tangible guide for the realization of these devices.

INDEX TERMS Substrate integrated waveguide, directional coupler, power divider T-type, computer simulation technology, microstrip transitions, waveguide.

I. INTRODUCTION

Power distribution networks play a pivotal role in dividing and combining signals, offering equal or arbitrary output signals to output ports with predetermined amplitude and phase. These networks find extensive applications in various fields, including mobile and satellite communications, measurement equipment, and radar systems, especially in the microwave and millimeter-wave (mmWave) frequency ranges. The advancement of these components is fundamental for the progress of modern communications, leading to the continuous development of power distribution networks.

Although rectangular waveguide power distribution networks have been extensively researched and manufactured, their integration with planar circuits poses challenges due to their intricate tridimensional (3D) geometry. Alternative solutions have been proposed to address these challenges and enhance integration capabilities. Directional couplers,

The associate editor coordinating the review of this manuscript and approving it for publication was Feng Wei.

T-unions, and microstrip transitions in Substrate Integrated Waveguide (SIW) technology offer a promising solution by synthesizing the waveguide within a dielectric substrate [1]. This approach mitigates the complexities associated with the 3D geometry of traditional waveguides, facilitating easier integration with planar circuits. The adoption of SIW technology presents a viable path forward, providing a more efficient and practical solution to the integration challenges posed by traditional power distribution networks.

SIW devices are manufactured using standard printed circuit board (PCB) techniques based on a laminated dielectric substrate and metal vias to provide lateral confinement. However, one of the major limitations of SIW structures is related to the dimensions, losses, and leakage of signals in the transitions and the installation of SMA coaxial connectors, which depend on the operating frequency and the dielectric material. Although the use of dielectric substrates with high permittivity allows for reducing the interconnection and the cavity size, it usually has a detrimental effect on losses and leads to poor quality factors [2] and leaks the signal.

SIW technology is a virtual waveguide geometry meticulously designed through the incorporation of linear arrays of metalized cylinders (via holes) within the same substrate employed for the planar circuit. This approach constructs a metallic waveguide within the substrate, filled with a dielectric material, and engineered using planar technology. This design closely resembles older technologies, such as microstrip and coplanar configurations, which allow seamless integration into other circuits via transmission lines [3], [4], [5], [6], [7]. The integration-friendly nature of SIW technology, similar to established methodologies, enhances its compatibility and adaptability within broader circuit architectures.

Directional couplers are vital components for signal division and combination, often integrated into complex power distribution systems like beamforming networks. Their applications span various fields, including satellite communications and radar systems operating at microwave and mmWave frequencies, making them indispensable for modern communication systems. Over time, a diverse array of waveguide couplers has been developed within waveguide technology. However, a significant challenge lies in creating prototypes with a reduced weight, size, and volume, which proves difficult with conventional methods. In response, SIW technology emerged as a promising solution that enables the synthesis of waveguide structures within a dielectric substrate, offering opportunities for integration with other devices and technologies. The adoption of directional couplers in SIW represents a significant advancement. This approach not only addresses size and weight constraints but also facilitates seamless integration into modern communication systems [1].

Using SIW technology in the construction of truncated T-type power dividers guarantees efficient signal transmission by allowing wave reflection within the conductive walls and the dielectric substrate [8]. This reflective mechanism contributes to low losses per conductor, ensuring excellent transmission performance. SIW technology, designed to operate at high frequencies, facilitates the creation of compact designs that are easily modeled and seamlessly integrated. The properties of SIW, including reduced size and ease of modeling, make it an ideal choice for implementing truncated T-type power dividers, especially in applications demanding optimal performance and minimal signal loss. More specifically, truncated T-type power dividers find widespread usage in communication equipment due to their reciprocal nature, devoid of losses, except for one of its three ports which may exhibit a mismatch. Typically, this type of power divider is made using various technologies, with coaxial, waveguide, and, most frequently, microstrip technologies being predominant choices [3]. The versatility in manufacturing options underscores the adaptability of T-type truncated power dividers to different scenarios. Their recurrent use is driven by the inherent advantages of being lossless and reciprocal, making them a preferred choice in diverse applications.

In light of the above considerations, special emphasis must be placed on the selection of substrates and the manufacturing process. Common choices include the use of low-cost substrates such as FR4 [9] or higher-end alternatives such as Rogers RT/duroid 5870/5880. However, it is crucial to acknowledge that material losses, dielectric permittivity, and fabrication tolerances significantly impact performance metrics - including insertion losses, return losses, and network isolation - of microwave devices [10]. This underscores the critical role of careful substrate selection and precise manufacturing techniques in optimizing the overall efficiency and effectiveness of microwave devices.

In [3], a prototype of a six-port junction was meticulously manufactured and evaluated on a Rogers RT/duroid 5880 laminate substrate with a relative permittivity (ϵ_r) of 2.2. The findings revealed commendable performance metrics, with return loss at ports 1 (S_{11}) and 2 (S_{22}) consistently below 15 dB throughout the frequency spectrum (22 - 26 GHz). Furthermore, isolation levels at output ports, S_{21} and S_{53}, were reported to be -21 dB and -37 dB, respectively. The transmission coefficients, represented by the parameters S_{31} to S_{61} for port 1, exhibited a satisfactory level of 10 dB, with an average insertion loss of 4.5 dB. Similarly, for port 2, represented by parameters S_{32} to S_{62}, the transmission coefficients maintained a level of -10 dB, with an average insertion loss of 4 dB. In particular, these losses were attributed to signal leakage during the installation of SMA connectors. In [11], the authors investigated various waveguide structures within substrates, including SIW, and demonstrated practical circuit examples such as SIW transitions, dual-mode filters, and resonators for designing a 12 GHz oscillator. Their findings showcased an average insertion loss of 3.5 dB across these devices. In addition, [5] presents an overview of state-of-the-art devices that utilize

SIW technology, including active and passive circuits with various solutions. Their discussion highlighted challenges related to the modeling and design of SIW components without specifically addressing insertion losses. They introduced compact power dividers ranging from 1 to 4, 1 to 8, and 1 to 16 with chamfered bends, reporting an average insertion loss level of at least 3 dB in the simulation results. However, experimental validation was lacking, suggesting a potential increase in insertion loss in practical scenarios. In [6], the authors proposed a systematic approach for designing and modeling transition structures integrating microstrip lines (MSL) with SIW filters, achieving prototypes with a modest insertion loss of 3 dB. Finally, in [12], two types of mixed-mode magic-Ts are proposed, achieving out-of-/in-phase equal power divisions with high isolation, common-mode rejection, and compact size. The first type uses a microstrip T-junction and microstrip/slotline transition, while the second type employs a single-ended-to-balanced network and balanced-to-balanced network, both integrating asymmetric shorted-stub-loaded resonators for tunable passbands and improved selectivity. In addition, [13] presents a balanced-to-single-ended filter power divider (BTSE) using multilayer mixed-mode magic-T, achieving wideband out-of-phase and in-phase responses through GCPW to slotline transitions. By integrating a stub-loaded resonator (SLR), the designed FPD features high-selectivity differential-mode filtering with close-to-passband transmission zeros and high broadband common-mode rejection, with experimental results demonstrating its performance.

Despite the advancements in SIW technology, and to the best of our knowledge, some gaps persist in the literature. Specifically, there is a lack of comprehensive studies that address the design and implementation of directional couplers with equal power distribution, hindering the practical deployment of such crucial components in communication systems. Additionally, existing research often overlooks optimized designs for T-union and microstrip-to-SIW transitions across specific frequency bands, leaving a gap in understanding the most efficient signal transfer methods between different transmission mediums. Furthermore, the absence of empirical validation to compare the simulated and experimental results hampers the practical assessment of the proposed devices, highlighting the need for more comprehensive studies to evaluate the effects of material choices and fabrication processes. Moreover, a systematic design methodology for the T-union and microstrip to SIW transitions is lacking, limiting the efficiency of integration into communication systems. Lastly, the challenge of insertion losses in SIW devices remains largely unaddressed in the literature, emphasizing the need for practical solutions to ensure reliable signal transmission in real-world applications.

Motivated by knowledge gaps in the literature and the discussions mentioned above, the following aspects constitute the primary contributions of this work.

- An overview of the design and implementation of a 4×4 ports directional coupler with equal power distribution is provided.
- The designs of T-union and microstrip to SIW transitions are proposed, utilizing SIW technology optimized through the CST Microwave Studio suite. These devices are specifically tailored for several band frequencies.
- Comparisons are made between the simulated and experimental results, highlighting the effects resulting from the choice of materials and the fabrication process.
- A systematic design for T-union and microstrip to SIW transitions of 10.0 to 40.0 GHz is introduced. The optimization of these devices focuses on two objectives: minimizing the parameter S_{11} while maintaining S_{12} and S_{13} close to 3 dB / 0 dB, respectively.
- Due to the insertion loss at all the proposed devices, it presents at least 4.0 dB in the simulation results and 6.0 dB in the experimental results. Therefore, it is proposed to incorporate a basic circuit of an amplifier with an average gain of 15 dB to compensate for these losses.
- For the power divider, we introduce a two-part (vias) septum design to improve return loss al port 1. We also provide a table with all dimensions needed for designing power dividers that achieve a wide bandwidth. By using the initial dimensions of standard rectangular waveguides and converting them to SIW waveguide devices, we achieve an available bandwidth of at least 20% in all power dividers.
- For the SIW-to-microstrip transitions, we propose a table with dimensions for microstrip tapers transitioning to SIW waveguides. This approach ensures an available bandwidth of at least 20% in all SIW-to-microstrip transitions.

This paper presents a schematic design process for multiple power distribution networks. The work is organized as follows to effectively illustrate this process. In Section II, an overview of the theory and design of a directional 4×4 port with arbitrary power distribution using SIW technology is presented. Furthermore, in the same section, the design process of a T-union power divider considers several standard waveguides from WR-90 to WR-28 covering low-band V-band frequencies. The developed prototypes and the results of the tests conducted are presented in Section III. Finally, the main conclusions are presented in Section IV.

II. THEORY AND DESIGN

In this section, we present the design of two distinct power distribution networks and a microstrip-to-SIW transition. The first new design involves a 4-input $\times$ 4-output directional coupler crafted with SIW technology, derived from a previous design for standard rectangular waveguides operating within the Ku band. Additionally, we explore several T-junction new designs employing SIW technology, optimized for frequencies ranging from the low end of the V-band (10 GHz)

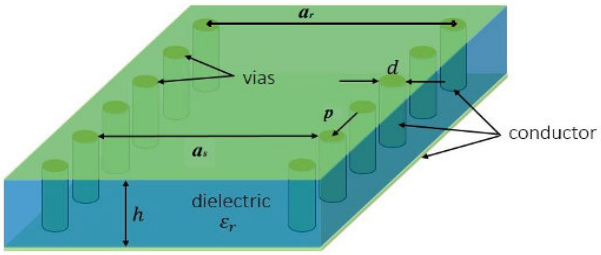

FIGURE 1. Key geometric parameters utilized in the design of SIW technology.

to 40 GHz. Furthermore, we investigate several microstrip-to-SIW transitions tailored for operation within the same frequency range on the basis of the design of a directional coupler based on rectangular waveguide theory. Furthermore, the design of the T-junction divider is based on the theory of the T-junction in rectangular waveguide technology, and finally, the dimensions of microstrip transitions are based on the theory in microstrip technology.

A. SIW RECTANGULAR GUIDE DESIGN

SIW technology uses a metallic waveguide constructed with linear arrays of metalized cylinders integrated into the same substrate used for the planar circuit and filled with a dielectric material, as illustrated in Fig. 1. The main parameters for the design are the diameter of the tracks, d, the spacing between tracks, p, the distance between the centers of the metallic track arrangements, a_r, and the effective SIW width, a_s, which must meet the following conditions as specified in [5], [11], [14], [15], and [16]:

$$d < \frac{\lambda_g}{5},\ p \leq 2d,\ a_r = \frac{a}{\sqrt{\varepsilon_r}},\ a_s = a_r - \frac{d^2}{0.95p}, \tag{1}$$

where λ_g is the cutoff frequency of the dominant mode TE_{10}, a denotes the value of a standard rectangular guide, and ε_r is the relative constant of the dielectric [5], [14], [17].

The cutoff frequencies of the 4×4 directional coupler are determined by meticulous analysis that takes advantage of the structural insights outlined in [18]. In the following, $f_{c,\mathrm{SIW}_{10}}$ is the cutoff frequency of the mode $\mathrm{TE}_{\mathrm{SIW}_{10}}$ in the SIW waveguide and $f_{c,\mathrm{SIW}_{20}}$ is the cutoff frequency of the mode $\mathrm{TE}_{\mathrm{SIW}_{20}}$. Thus, this analysis employs that

$$f_{c,\mathrm{SIW}_{10}} = \frac{c}{2\sqrt{\varepsilon_r}}\left(a_s - \frac{d^2}{0.95p}\right)^{-1}, \tag{2}$$

and that

$$f_{c,\mathrm{SIW}_{20}} = \frac{c}{\sqrt{\varepsilon_r}}\left(a_s - \frac{d^2}{1.1p} - \frac{d^3}{6.6\,p^2}\right)^{-1}. \tag{3}$$

In addition, the wavelength of a rectangular guide is calculated as

$$\lambda_{s,\mathrm{TE}_{10}} = \frac{\lambda_0/\sqrt{\varepsilon_r}}{\sqrt{1-(f_{c,\mathrm{SIW}_{10}}/f_0)^2}}, \tag{4}$$

where λ_0 and f_0 denote the wavelength and central frequency, respectively.

B. DIRECTIONAL COUPLERS WITH EIGHT PORTS

The initial step in designing a 4×4 port directional coupler involves crafting the directional coupler within a rectangular waveguide framework. This coupler typically comprises two symmetrical planes, as illustrated in Fig. 2, with input and output ports meticulously matched and isolated. Once the design within the rectangular waveguide is established, the next phase entails translating this configuration into SIW technology. This transformation is achieved by using relevant equations to ensure equivalence between the rectangular waveguide and the SIW structures. Notably, an accurate specification of parameters pertaining to the appropriate RT Duroid material, including the dielectric constant and loss tangent, is imperative to initiate the calculation effectively.

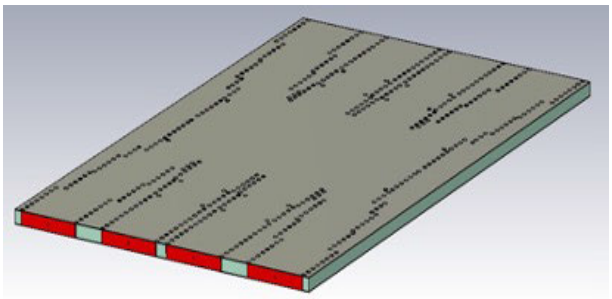

FIGURE 2. Layout design of the 4 × 4 Port Directional Coupler using RT-DUROID 5880.

Once the parameters for the rectangular waveguide in the SIW have been determined, the structure is proportionally scaled to match the corresponding width of the guide in SIW. Subsequently, the central plate of the RT Duroid 5880 substrate is incorporated with a height of $h = 1.57$ mm, as specified in the electrical specifications of the substrate. Following this, the upper and lower plates of perfect electrically conductive (PEC) material are added with a thickness of 0.1 mm each. To complete the setup, the directional coupler is encased within a metal casing with a diameter of 0.6 mm and a center-to-center distance of 1.2 mm. Fig. 3 shows the final dimensions considering the transition in each port in the directional coupler in the SIW technology.

According to the design specifications, the waveguide standard for the coupler is WR-51 [19], with dimensions $a = 12.954$ mm and $b = 6.477$ mm, operating at a frequency of 16.5 GHz. Based on these parameters, the cutoff frequencies for the dominant propagation modes, namely TE_{10} and TE_{40}, are calculated as follows [20]:

$$f_{c,\mathrm{TE}_{10}} = \frac{c}{2a} = 11.579\ \mathrm{GHz} \tag{5}$$

$$f_{c,\mathrm{TE}_{40}} = \frac{2c}{a} = 46.318\ \mathrm{GHz} \tag{6}$$

Within this cut-off frequency range, the coupler operates effectively within the desired frequency and bandwidth parameters. Once the frequencies of the dominant modes

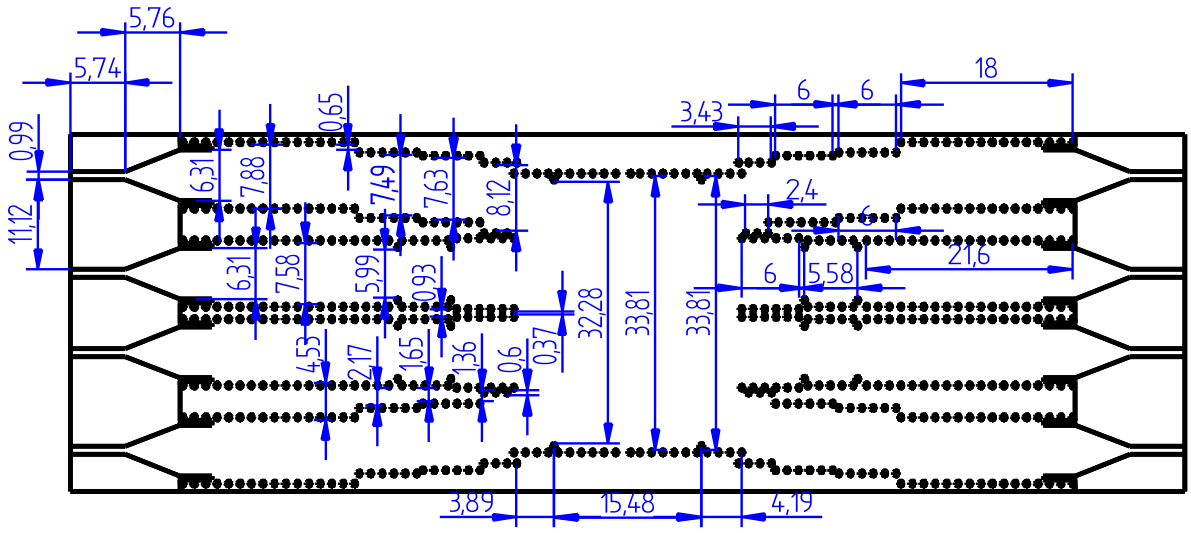

FIGURE 3. Directional coupler eight-port design.

have been determined, their propagation constants are computed using [20]:

$$\beta_{\mathrm{TE}_{10}} = \sqrt{\gamma^2\mu\epsilon - \frac{\pi^2}{w^2}} = 579.746\ \mathrm{m}^{-1}, \tag{7}$$

$$\beta_{\mathrm{TE}_{40}} = \sqrt{\gamma^2\mu\epsilon - \frac{4\pi^2}{w^2}} = 460.480\ \mathrm{m}^{-1}, \tag{8}$$

where μ and ϵ are permeability and permittivity, respectively.

Let the subscripts e and o represent the symmetries with constants β_e and β_o, respectively. Thus, β_e and β_o are the propagation constants in even and odd analysis on the directional coupler. The difference between them results in the approximate length of the central cavity or coupling region. These values depends of propagation modes TE_{40} and TE_{10}. Taking into account these propagation constants, we estimate the value of L, that is, the length of the central cavity of the directional coupler, using the following power ratio [20]

$$(\beta_{\mathrm{o}} - \beta_e)\frac{L}{2} = \tan^{-1}(r). \tag{9}$$

The proposed coupler, shown in Fig. 2, utilizes SIW technology. For the analysis and design, the structure was divided into several building blocks, described as follows. The ports were standard rectangular waveguides, with WR-XX used for any frequency band. The dimensions were in millimeters, with a_{siw} representing the width and b representing the height of the substrate, which in this case is specified as ROGERS RF5880.

Routing arms with discontinuities in the SIW waveguide width were employed to transfer the signal from the input ports to the coupling region. These elements were designed to achieve equal transmission to all output ports. According to the layout in Fig. 2, this required the magnitudes of $S_{j,1}$ and $S_{j,2}$ (with $j = 5, \ldots, 8$) to be close to -6 dB, while keeping isolation $S_{j,1}$ (for $j = 2, 3, 4$) and $S_{j,2}$ (for $j = 1, 3, 4$) as low as possible.

Given the two-fold symmetry of the directional coupler, it could be divided into four equal parts, simplifying the network analysis. The other S-parameters were derived through symmetry. Specifically, considering the coupler symmetries shown in Fig. 2, the analysis was reduced to two-port structures with appropriate boundary conditions of a perfect electric wall and a perfect magnetic wall in the planes AA' and BB' [21].

For the design of the coupler, the structure was initially divided into two main parts: the routing arms and the coupling region. Due to the symmetry of the coupler, Port 1 is equivalent to Ports 4, 5, and 8, while Port 2 is equivalent to Ports 3, 6, and 7. The routing arms for Port 1 consist of several off-center blocks, whereas those for Port 2 are composed of several blocks and irises. The initial dimensions of the routing arms were based on the six-port coupler described in [22].

Next, the connection of the $N = 8$ routing arms from the coupler ports, as shown in Fig. 2, was achieved through a coupling region with an initial width equal to $a_{\mathrm{siw}} \times \frac{N}{2}$, where a_{siw} is the width of the SIW waveguide of the ports. Thus, the initial width was 23.3 mm, allowing the propagation of the higher-order mode TE_{40} in this coupling region.

Finally, the dimensions of the routing arms and the coupling region were optimized to meet the electrical specifications shown in Table 1. The design's central frequency was set to 16.5 GHz, with a bandwidth of 1 GHz with a

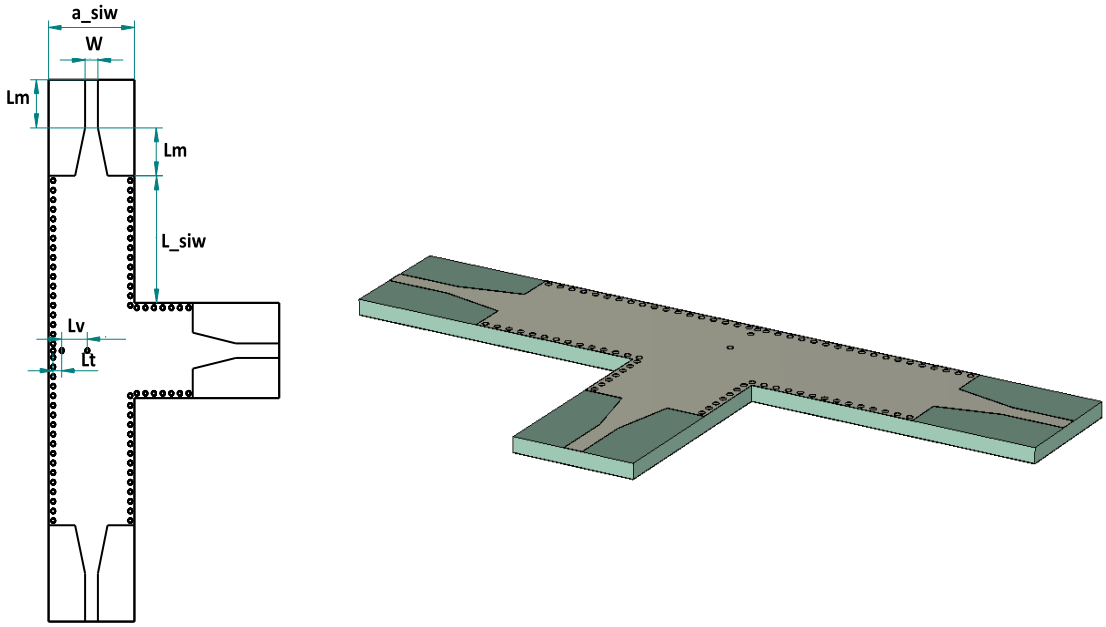

FIGURE 4. T-Type power divider. Left: front view, Right: perspective view.

TABLE 1. Electrical specifications of directional coupler.

Parameter	Value
a_{siw}	7.58 mm
Operation frequency	16 - 17 GHz
Ports in	4
Percentage bandwidth	5%
Ports out	4
Interface	2.3 mm
Return loss	< 15 dB
Isolation	< -15 dB
Coupling	-6.02 ± 1 dB

frequency band frequency range of 6% and a return loss level of 15 dB [21].

C. T-TYPE DIVIDER DESIGN

Fig. 4 shows the proposed structure, highlighting all parameters relevant to the design of the T-junction. The T-Type power divider consists of two branches of identical length linked to a single input port and two output ports. The parameters used to construct the T-type junction are outlined on the left side of Fig. 4, and the dimensions of the rectangular waveguide ports are detailed in Table 2. WR-XX are standard waveguides that define the cutoff frequency of TE_{10} and TE_{20} and the dimensions that are used by many manufacturers for this kind of device. Table 2 shows the parameters considered in the design of the divider. a_{siw} in the width of the SIW waveguide, L_{m1}, and L_{m2} are the length of the microstrip transition. L_{siw} is the length of the SIW output ports, and L_v and L_t are the dimensions in the septum that are used to improve S_{11}.

A septum incorporated into the T-type power divider facilitates a uniform distribution of the input wave. Furthermore, when waveguide technology is employed, the septum can adopt a triangular or square shape. In such instances, the septum comprises two offsets strategically positioned to enhance the return loss of Port 1. An additional via was added to the substrates to assess the response of the divider, as shown in Fig. 5. From this figure, it is evident that the truncated T-Type power divider operates at the central frequency of the rectangular waveguide, with the signal at its output ports hovering around -3dB. The width bandwidth extends to 3500 MHz, covering approximately 22.51% of the entire bandwidth.

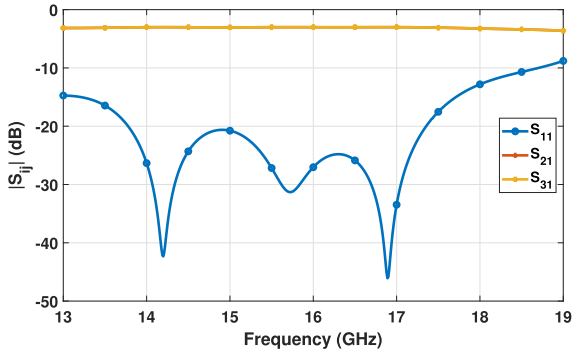

FIGURE 5. S-parameters from T-Type power divider with a_{siw} from WR62 standard rectangular waveguide.

In our endeavor to design a three-way truncated T-type power divider accommodating various rectangular

TABLE 2. Basic parameters for T-type union.

RWG-ST	a_{siw} (mm)	W (mm)	L_{m1} (mm)	L_{m2} (mm)	L_v (mm)	L_t (mm)	L_{siw} (mm)
WR-90	14.85	5	8	6.04	3.1	1.7	20.5
WR-75	10.40	3.5	10.0	14.01	2.9	1.5	18.4
WR-62	10.10	1.8	6.0	6.15	2.95	0.6	15.6
WR-51	7.0	3.5	8.0	7.75	1.90	0.58	13.8
WR-42	5.63	3.5	8.1	6.01	1.40	0.52	7.61
WR-34	6.4	2.8	6.7	6.52	1.85	0.47	11.35
WR-28	7.29	3.5	4.55	5.75	1.20	0.16	6.6

waveguide dimensions, ranging from standard rectangular waveguides WR-90 to WR-28, we initially crafted a single rectangular SIW waveguide optimized for a specific center frequency. To achieve this, we adhere to design principles centered around the diameter d being the same as used in the previous section. Furthermore, b is the distance between biases in SIW technology. Likewise, the periodicity of the distances b between each hole is crucial. This consideration is paramount because the arrangement of holes mimics and simulates the sidewalls of a conventional rectangular waveguide; opting for excessively large values could lead to signal leakage and increased signal losses. Therefore, it is advisable to employ values of $d = 0.6$ mm and $b \leq 1.2$ mm for standard frequencies or $d = 0.4$ mm and $b \leq 0.8$ mm for higher frequencies, respectively.

After determining the intrinsic parameters of the SIW waveguide, the next step involves identifying the parameters corresponding to the frequency bands of interest. These include the SIW wavelength, λ_{SIW}, the effective width of the SIW waveguide W_{SIW}, which correlates directly with the operational frequency, and the mode of wave propagation. The length of the rectangular waveguide is set to $\lambda/2$ to ensure seamless integration with the original wave, thus minimizing substrate losses and validating the design's functionality within the operational band, with a center frequency contingent upon the waveguide dimensions.

Following the design and simulation of the conventional waveguide, the dielectric substrate to implement the SIW waveguide undergoes adaptation. We opted for the RF5880 substrate, which is readily available and capable of supporting frequencies up to 40 GHz. In the process of designing and simulating the waveguide, the new waveguide width a_{SIW} is calculated within the substrate using the dielectric constant, producing values as specified in the second column of Table 2. When transitioning from the traditional substrate waveguide to SIW, we leverage the intrinsic parameters previously obtained from the optimization process in each divider prototype to perform the SIW transformation.

The SIW technology inherently operates solely in the TE_{m0} propagation mode due to its nature and structure [4], [15]. Consequently, the effective wavelength differs from that which propagates in a vacuum. Thus, the cutoff frequency formulas given in (1) and (2) are applied in this propagation mode to obtain $f_{c,\text{SIW}_{10}}$ and $f_{c,\text{SIW}_{20}}$, respectively. Using these values and employing (4), we can derive $\lambda_{s,\text{TE}_{10}}$ for all standard waveguide dimensions.

Subsequently, with the parameters for the SIW waveguide determined, the base design of the divider is structured, incorporating the design of the septum and transitions at a coupling distance. The scattering parameters are then obtained using the full-wave CST Microwave Studio software tool, as illustrated in Figs. 5 and 7. In the figures, the blue curves represent the S_{11} parameter, which maintains a level of less than 20 dB throughout the frequency band. This indicates excellent impedance matching and minimal reflection, which is crucial for efficient signal transmission. The orange and red curves represent the transmission coefficients, each showing a 3 dB level due to the two output ports in the divider. This consistent 3 dB split confirms the effective power distribution between the output ports, ensuring balanced signal strength in both paths.

The other parameters in Table 2 crucial for the design of the T-junction include the transition width W, designed to accommodate the 50 Ω SMA connector, and L_{m1}, representing the length of the first section of the transition. The transition consists of two sections, with the second section characterized by a width L_{m2}. To enhance the return loss at Port 1, the septum is composed of two vias, defined by the parameters L_v and L_t. L_v is the distance from the main SIW waveguide of the divider to the first via of the septum, while L_t is the distance from the first via to the second via. These parameters are optimized to ensure that at least 10% of the available bandwidth is reached.

Another critical dimension to consider is the length of ports 2 and 3, denoted as L_{siw}. This parameter allows for flexibility in the optimization process, ensuring an equal distribution of power among the ports. These parameters collectively contribute to the construction of the three-port divider for each standard rectangular waveguide dimension, ranging from WR-28 up to WR-90. Table 2 presents the optimized final dimensions of these parameters.

D. SIW WAVEGUIDE TO MICROSTRIP TRANSITION DESIGN

The design of the taper transition [6], [17], [23], [24], [25] was facilitated with the assistance of LineCalc from the Keysight calculator. This tool utilizes the RF-5880 parameters and the operational frequency to generate a microstrip line with

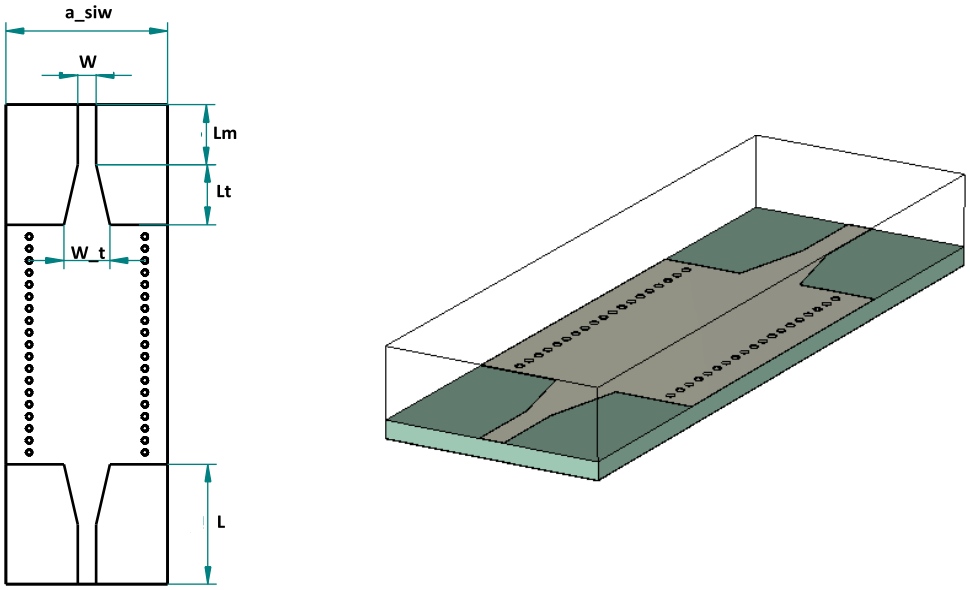

FIGURE 6. Geometry for the taper and microstrip transitions design.

dimensions: waveguide width (a_{siw}), taper width (W), and a two-section taper with lengths L_t and L_m. Furthermore, the width of the tapered microstrip at the beginning of the transition waveguide (W_t) is determined to achieve an impedance value of 50 Ω and a phase shift of 180°. In particular, the width W_t is chosen to achieve an impedance of 50 Ω, which is a standard impedance for many RF and microwave applications, and the phase shift of 180° is often necessary for applications such as signal modulation, phased arrays, and certain types of filters.

Subsequently, a trapezoid was incorporated into the SIW device, allowing the calculation of the width and length of the tap trapezium considering the following

$$W_t \approx 0.4\, a_{\text{siw}}, \tag{10a}$$

$$\lambda_s/2 < L_t < \lambda_s. \tag{10b}$$

Fig. 6 shows the geometry for the design of the taper and microstrip transitions. Here, the tap values underwent adjustments via two-variable parametric optimizations to attain the optimal transition response. The final values of all parameters are presented in Table 3, which presents the optimized dimensions of the SIW-Microstrip transition after considering several standard rectangular waveguide dimensions, ranging from WR-90 to WR-22.

III. PROTOTYPES DEVELOPED AND RESULTS

This section compares the simulation results with the experimental results of the three prototypes manufactured. The experimental results were obtained with the network analyzer and low-loss cables. The prototypes under test were the eight-port directional coupler, three T-junction dividers, and three microstrip lines to the SIW waveguide. The comparison between results shows similar behavior. In addition, we propose a scheme to improve the loss in the substrate using a wideband amplifier.

TABLE 3. Design parameters for microstrip to SIW transition.

RWG-ST	a_{siw} (mm)	W (mm)	L_m (mm)	L_t(mm)	W_t(mm)
WR-90	14.85	5.00	8.00	6.04	6.40
WR-75	13.75	3.10	10.0	14.33	7.0
WR-62	10.70	1.80	6.0	6.15	4.50
WR-51	8.99	5.40	8.0	8.06	3.50
WR-42	6.88	4.27	16.7	6.50	3.69
WR-34	6.40	2.80	6.7	6.52	3.69
WR-28	6.58	3.50	14.0	5.80	3.84

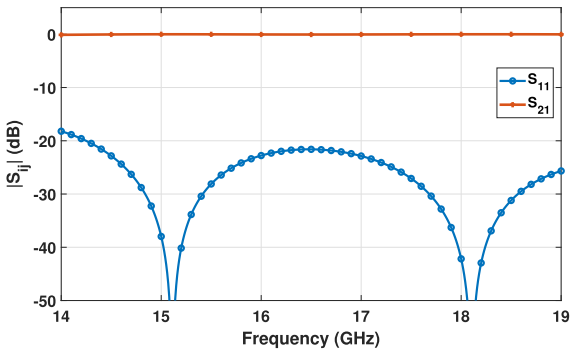

FIGURE 7. S parameters simulations results of WR62 transitions.

A. EIGHT PORT DIRECTIONAL COUPLER PROTOTYPE

To achieve the results presented, we utilized CST Microwave Studio software to simulate and optimize real lumped

FIGURE 8. Eight-port directional coupler manufactured in SIW technology.

components and substrate materials. In addition, to validate our findings, we conducted scattering parameter measurements on prototypes fabricated with microstrip technology. This verification process was carried out using a Keysight N9918A FieldFox Handheld Microwave Network Analyzer, spanning frequencies from 10 to 20 GHz.

The prototype of the directional coupler is shown in Figs. 8 and 9. The 4 × 4 directional coupler was manufactured on an RF-5880 substrate, adding to the microstrip transition of the ports and the SIW waveguide at each port to achieve the objective of obtaining experimental results using a network analyzer. The 4 × 4 Ku-band directional coupler, employing SIW technology, was meticulously crafted and refined using the CST Design program. Due to its symmetrical configuration, the outputs of Port 1 are equivalent to those of Ports 4, 5, and 8, while Port 2 aligns with Ports 3, 6, and 7.

FIGURE 9. Eight-port directional coupler manufactured in SIW technology with SMA connectors.

Fig. 10 shows the S parameters from port 1. The blue curve represents S_{11}. The return loss level is less than 15.0 dB between frequencies 15.65 GHz and 16.61 GHz. The dashed curves represent S_{12}, S_{13}, and S_{14}, which are the isolation parameters of the directional coupler for ports 2, 3, and 4, respectively. Considering the properties of this network, like symmetry, reciprocity, and losslessness. These parameters exhibit isolation levels better than 15.0 dB in almost all frequency bands. The curves green S_{51}, white blue S_{61}, purple S_{71} and S_{81} pink show the transmission coefficients, respectively, that have a magnitude level of -6.03 ± 1.5 dB.

Fig. 11 shows the S parameters from port 2. The red curve represents S_{22}. In this case, the return loss level is less than 15.0 dB between the frequencies 16.16 GHz and 16.42 GHz. The dashed curves represent S_{21}, S_{32}, and S_{42}, which are the isolation parameters of the directional coupler for ports 2, 3, and 4, respectively. These parameters exhibit isolation levels better than -15.0 dB across almost all frequency bands. The green curve (S_{52}), the light blue curve (S_{62}), the purple curve (S_{72}), and the pink curve (S_{82}) represent the transmission coefficients, which have magnitude levels of -6.03 ± 1.5 dB.

In Figs. 10 and 11, a noticeable increase in insertion losses is evident at both port 1 and port 2. This rise primarily originates from inadequately metalized pathways, leading to distorted wave propagation and incorrect transport to the output port, compounded by losses incurred during the soldering of the SMA connectors. In addition, the effect of the depth of the skin plays a role in determining the depth of penetration of the wave into the material. In this case, the skin depth is insufficient, causing waves to escape the dielectric and resulting in significant losses. To counteract these insertion losses, it is crucial to ensure proper pathway metallization, use high-quality soldering techniques for SMA connectors, and select materials with suitable skin depths to minimize wave leakage.

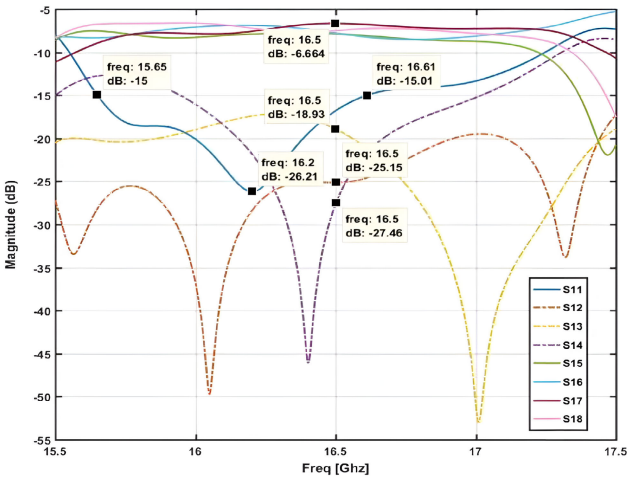

FIGURE 10. Eight-port directional coupler S-parameter port 1, experimental results.

The insufficient thickness of the metal tracks' walls failed to adequately confine the waves within the dielectric material, resulting in the observed losses. Consequently, the bandwidth decreased significantly from 960 MHz to 210 MHz, as shown in the blue curve S_{11} and red curve S_{22} in Figs. 10 and 11, respectively, attributable to construction errors and incomplete metallization of the cylinders. As a result, the peak working frequency experienced a displacement of 0.36 GHz. This discrepancy may stem from slight variations in the final width of the guide post-fabrication, as even minute changes in dimensions can induce shifts in the operating

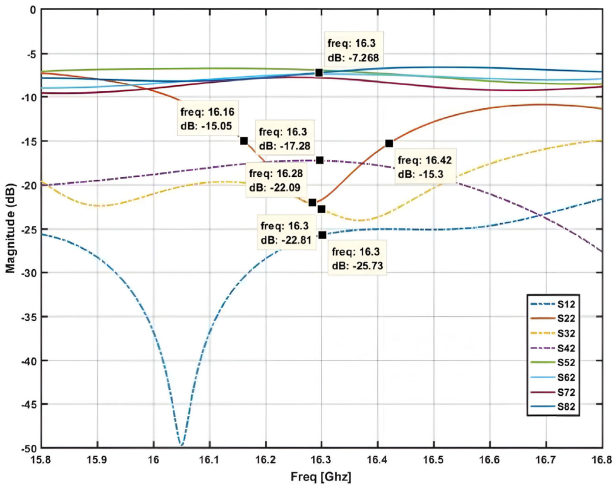

FIGURE 11. Eight-port directional coupler manufactured S-parameter port 2, experimental results.

frequency. Moreover, inadequate track metallization further exacerbates losses in the electromagnetic waves traversing the dielectric.

The directional coupler, grounded in research in SIW technology, boasts several advantageous features. In particular, it has high integration density, cost-effectiveness in comparison to traditional waveguides, and the creation of inexpensive devices. Its compact size contributes to reduced weight and seamless integration into microwave systems. However, because of its diminutive dimensions, manufacturing demands meticulous precision. Even minute inaccuracies in construction, down several millimeters, can lead to significant losses.

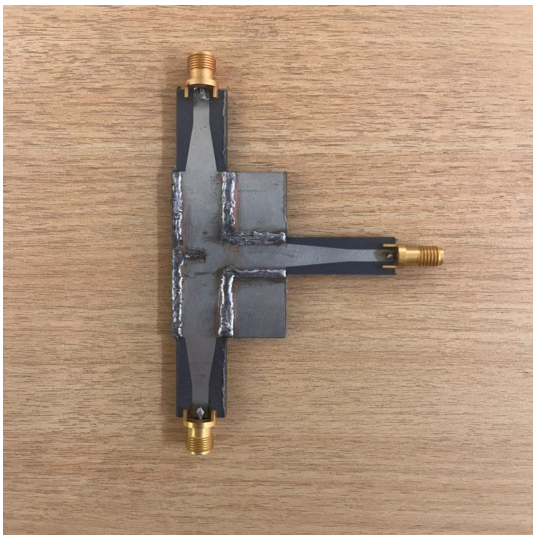

FIGURE 12. T-type power divider WR-75.

The experimental results of isolation at the directional coupler for port 1 are presented in Fig. 10, represented by dotted curves. The red curve shows the experimental result of the S_{12} parameter with a level of less than -20 dB between 15.5 and 17.5 GHz, the yellow curve presents the experimental result of the S_{13} parameter with a level of less than -18 dB between 15.5 GHz and 17.5 GHz, and finally, the purple curve illustrates the S_{14} parameter with a level of less than -15 dB between 16 and 17 GHz. It is known that this directional coupler has or presents two symmetry axes and has reciprocity, therefore the $S_{ij} = S_{ji}$ considering reflection coefficients, isolations parameters, and transmission coefficients, then $S_{12} = S_{21}$, $S_{13} = S_{31}$ and $S_{14} = S_{41}$ for the isolation parameters.

The experimental results of isolation at the directional coupler for port 2 are presented in Fig. 11, represented by dotted curves. The red curve shows the experimental result of the S_{21} parameter with a level of less than -20 dB between 15.5 and 17.5 GHz, the yellow curve presents the experimental result of the S_{32} parameter with a level of less than -15 dB between 15.5 and 17.5 GHz, and finally, the purple curve illustrates the S_{42} parameter with a level of less than -15 dB between 15.5 and 17.5 GHz.

Due to the coupler symmetry, port 1 is equivalent to ports 4, 5, and 8, while port 2 is equivalent to ports 3, 6, and 7. Considering this property, we present the results for port 1 and port 2 in Fig. 10 and Fig. 11, respectively. The device is fully characterized by only two ports due to symmetry.

The experimental results demonstrate that the couplers achieve high isolation across the specified bandwidths, with the S_{21} parameter showing isolation levels of less than -20 dB between 15.5 and 17.5 GHz for both port 1 and port 2. Consistent isolation levels below -15 dB for multiple S-parameters indicate effective signal isolation across different paths. The consistent isolation performance observed validates the design's symmetry, confirming that the design effectively mitigates signal interference and crosstalk, crucial for applications requiring high signal integrity.

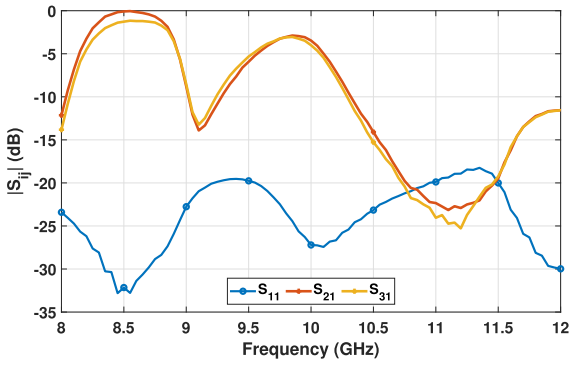

FIGURE 13. S parameters experimental results T-type power divider WR-75.

B. T-TYPE POWER DIVIDER EXPERIMENTAL RESULTS

Fig. 12 shows the completed prototype of the divider WR-75, including the SMA connectors used to link with

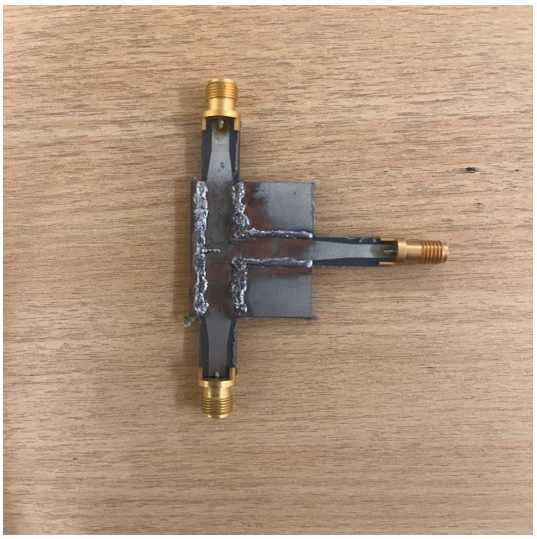

FIGURE 14. T-type power divider WR-62.

the network analyzer. Fig. 13 illustrates the experimental results for the parameters S_{11}, S_{21}, and S_{31} of the T-type divider with microstrip transitions. More specifically, the blue curve represents the response S_{11}, while the red and yellow curves denote the transmission coefficient responses S_{21} and S_{31}, respectively. The scattering parameters demonstrate commendable performance, attaining values close to -3 dB at the output ports, indicative of a halving of the input power. Furthermore, the return loss parameter S_{11} exhibits a response between 9 and 11 GHz with levels below 20 dB, centered around 10 GHz. These characteristics establish the device as an exemplary T-type power divider with an available bandwidth percentage of 18.0%.

Fig. 14 shows the prototype of the WR-62 divider manufactured with SIW. The scattering parameters of the divider, presented in Fig. 15, demonstrate good performance. Specifically, the output ports S_{21} and S_{31} exhibit a transmission coefficient near -5.0 dB, indicating efficient power division (halving the input power). The return loss parameter, S_{11}, shows a response centered around 14.5 GHz with values below 20 dB between 13 and 16 GHz. These characteristics establish the device as a truncated T-type power divider with a usable bandwidth exceeding 20%.

Fig. 16 shows the prototype of the divider WR-51. The scattering parameters in Fig. 17 demonstrate interesting performance, reaching a value close to -6 dB at the output ports, signifying a division of the input power by half. Furthermore, the return loss parameter S_{11} exhibits a response between 15.5 and 18 GHz with levels below 20 dB, centered around 16.25 GHz. These characteristics establish the device as an ideal truncated T-type power divider with an available percentage bandwidth of 15%.

Fig. 18 shows the simulation results of isolation at port 1 of the power divider, represented by the blue and red curves. The blue curve indicates the simulation result for the S_{32} parameter, and the red curve for the S_{23} parameter,

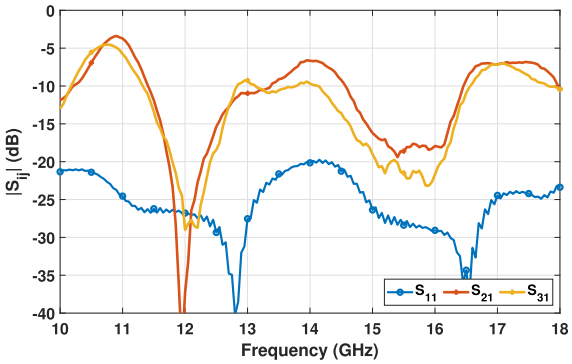

FIGURE 15. S parameters T-type power divider WR-62 (experimental results).

FIGURE 16. T-type power divider WR-51.

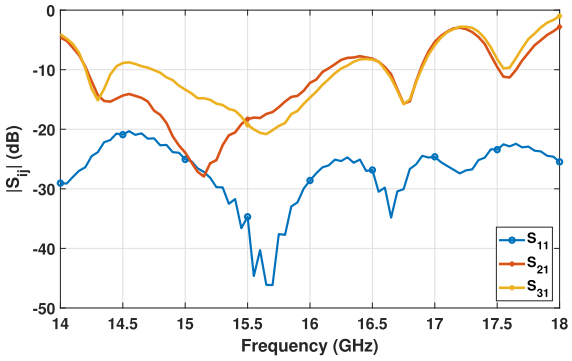

FIGURE 17. S parameters T-type power divider WR-51 (experimental results).

both demonstrating isolation levels below -7.5 dB between 14 GHz and 19 GHz.

Fig. 19 presents the simulation results of isolation at port 2 of the power divider, also represented by the blue and red curves. The blue curve shows the simulation result for the S_{32} parameter and the red curve for the S_{23} parameter, both

indicating isolation levels below −6.0 dB between 8 GHz and 12 GHz.

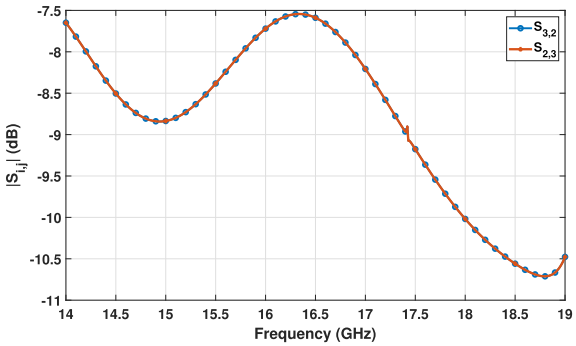

FIGURE 18. S parameters of isolation from T-type power divider WR-62 (experimental results).

These simulation results highlight the effective isolation performance of the power dividers across the specified frequency ranges. The isolation levels achieved are satisfactory for practical applications, ensuring minimal interference between the output ports. This performance indicates that the design is robust and can maintain high isolation, which is critical for the efficient operation of power dividers in high-frequency systems.

C. SIW-MICROSTRIP TRANSITION

Fig. 20 shows the final prototype of the transition WR-75, and Fig. 21 displays the experimental results of the network, with the blue curve representing the response S_{11} and the red curve representing the transmission coefficient result S_{21}. The scattering parameters exhibit favorable behavior, with the output port achieving a value close to −3 dB, indicative of a successful signal passage. Furthermore, the return loss parameter S_{11} shows a response between 9 and 12 GHz, with levels below 20 dB and a central frequency of 10.5 GHz, making this device a transition with a generously available percentage bandwidth of 30%.

Fig. 22 shows the final prototype of the transition WR-62. As can be seen in Fig. 23, the scattering parameters exhibit reasonable behavior, with the output port achieving a value close to −3 dB, indicating successful signal transmission. Furthermore, the return loss parameter S_{11} demonstrates a response between 11.0 and 14.0 GHz, with levels below 20 dB and a central frequency of 12.5 GHz. These characteristics classify this device as a transition with an available percentage bandwidth of 24%.

Fig. 24 shows the final prototype of the WR-51 transition. The scattering parameters demonstrate the performance illustrated in Fig. 25, with the output ports achieving a value close to −4 dB. Furthermore, the return loss parameter S_{11} exhibits a response between 15.5 and 18.5 GHz, with levels below 20 dB and a central frequency of 16.0 GHz. These characteristics classify this device as an SIW transition with an available percentage bandwidth of 18.7%.

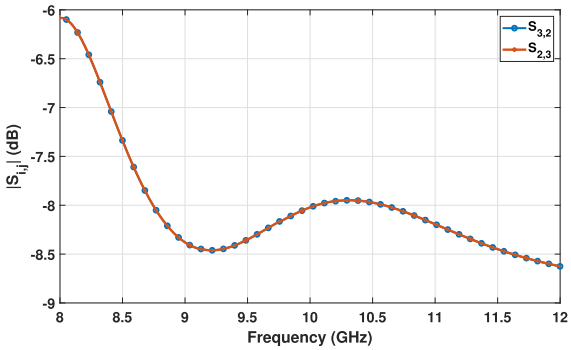

FIGURE 19. S parameters of isolation from T-type power divider WR-75 (experimental results).

FIGURE 20. SIW microstrip transition WR-75.

The variations in amplitude in our results can be attributed to a few factors. Insufficiently metalized pathways may have caused distorted wave propagation and incorrect signal transport. Additionally, soldering losses of the SMA connectors and insufficient skin depth, leading to wave escape from the dielectric, contributed to the losses. There was also minor signal leakage in the virtual walls of the SIW waveguide. These issues arose due to the specific laboratory conditions considered during our experiments. While the methodology used is not incorrect, the quality of the tools has a significant impact on high-frequency devices. The prototypes were developed in a laboratory environment, and these issues could potentially be resolved using more sophisticated and expensive tools. By improving the metallization process to ensure uniform and adequate coating of the vias and pathways, optimizing the soldering process of SMA connectors, and enhancing the precision in creating virtual walls in the SIW waveguide, it is possible to mitigate these problems and achieve better amplitude balance.

During the final manufacturing process of the prototypes shown in Figs. 12, 14, 16, 20, 22, and 24, notice that tin

TABLE 4. Comparison of SIW waveguide devices: Directional couplers, power dividers, and microstrip transitions.

Ref.	Bandwidth Percentage	Worst S_{11} (dB)	Coupling (dB)	Insertion Loss (dB)	Type of Device	Technology
[3]	16.6%	15.0	-6 ± 2.0	-4.5 ± 0.5	Six-port Junction	SIW
[5]	1.5%	10.0	0 ± 3.0	-7.3 ± 0.5	Power divider	SIW
[6]	5%	15.0	0 ± 1.5	-3.0 ± 0.5	Filter	SIW
[11]	3.5%	12.0	0 ± 1.5	-3.01 ± 0.5	Several devices	SIW
[12]	59%	10.0	-3 ± 1.21	-4.4 ± 0.5	Magic Tee	SIW and Microstrip
[13]	4.4%	10.0	-3 ± 1.21	-3 ± 0.5	Magic Tee	Microstrip
Our work	5%	20.0	-6 ± 2.0	-3.02 ± 1.0	Directional coupler	SIW
Our work	20%	20.0	-3 ± 3.0	-5.02 ± 1.0	Power divider	SIW
Our work	20%	20.0	0 ± 3.0	-5.02 ± 1.0	Transition	SIW and Microstrip

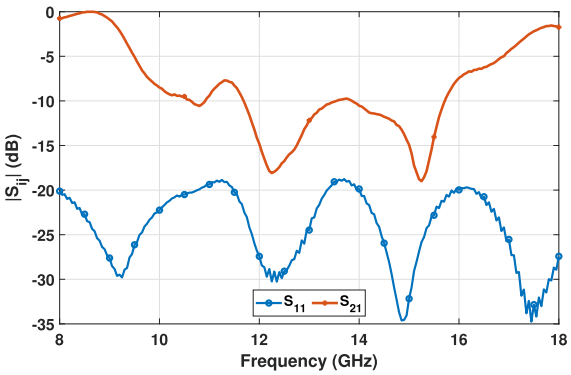

FIGURE 21. SIW microstrip of transition WR-75 (experimental results).

FIGURE 22. SIW microstrip transition WR-62.

soldering was added to improve the metalized process of the metallic posts in the SIW waveguides and the metalized pathways. This improves the correct skin depth at the virtual walls of the waveguides.

Despite the limited number of works addressing directional couplers, power dividers, and transitions from SIW waveguides to microstrip lines, we have developed and summarized a comparison of our results with other efforts in power distribution networks in Table 4. The comparison evaluates key parameters such as bandwidth percentage, return loss, coupling, insertion loss, device type, and technology. For the directional coupler, our work achieves an available bandwidth percentage of 5%, with an average isolation of −20 dB in ports 1 and 2. This demonstrates a simple structure with sufficient bandwidth and good performance. In the case of power dividers, our prototypes achieve at least 20% bandwidth, surpassing other works. This highlights the simple structure, excellent performance, and versatility of our layouts across different frequency ranges. The transitions from SIW waveguides to microstrip lines exhibit an excellent bandwidth percentage of 20%, featuring simple structures and robust performance. Although the insertion losses in our prototypes are slightly higher, Table 4 shows that the overall behavior and performance of our designs are comparable to, or even better than, those of other high-performing devices in certain aspects. These results underscore the effectiveness of our designs in delivering high-performance devices with straightforward structures and broad bandwidth capabilities.

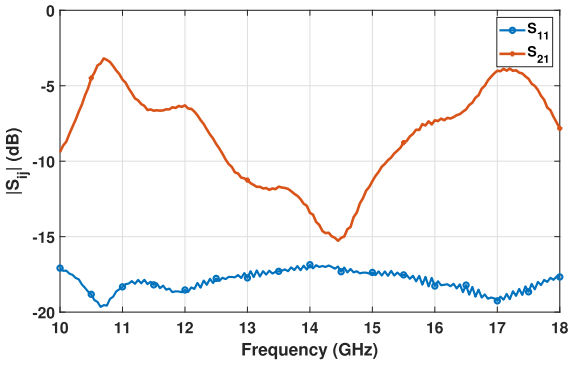

FIGURE 23. SIW microstrip of transition WR-62 (experimental results).

D. INSERTION LOSSES AT THE SUBSTRATE

The prototypes were manufactured using the RF-5880 substrate. Thus, the insertion loss in the devices is at least 3 dB due to the microstrip transition. Previous works have indicated that this type of device experiences losses due to SMA connectors and signal leakage. Therefore, it is necessary to add an active device, such as a monolithic

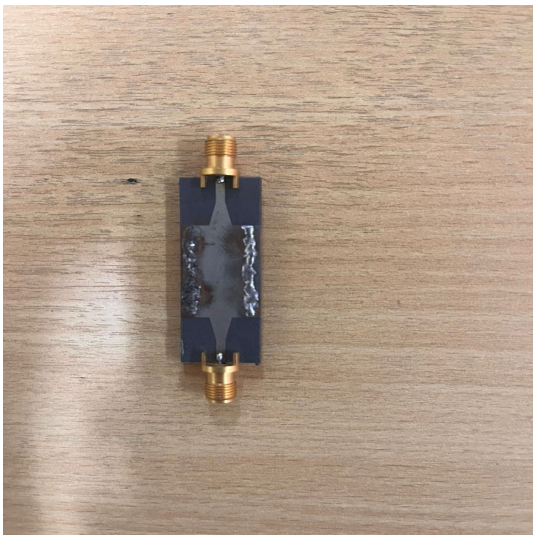

FIGURE 24. SIW microstrip transition WR-51.

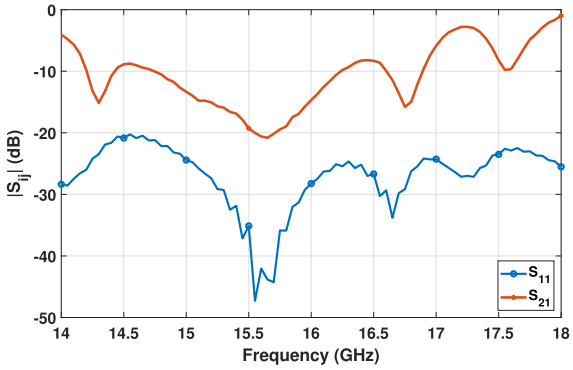

FIGURE 25. SIW microstrip transition WR-51 (experimental results).

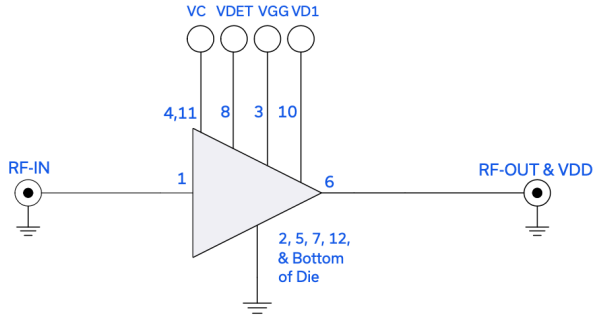

FIGURE 26. MMIC amplifier AVA-054-D+ schematic [26].

microwave integrated circuit (MMIC) amplifier. The Mini-Circuits AVA-054-D+, with a bandwidth from DC to 50 GHz, is suitable for this purpose. This amplifier can be used in a_{siw} from WR-90 to WR-28 to compensate for insertion losses. Fig. 26 shows the basic pin scheme of the amplifier, and Fig. 27 depicts the basic circuit for implementation.

Fig. 28 shows the S-parameters of the amplifier. The return loss, S_{11} (blue curve), is 15 dB throughout the bandwidth. The reflection coefficient of port 2, S_{22} (purple curve), is also shown. The gain of the amplifier, S_{21} (red curve),

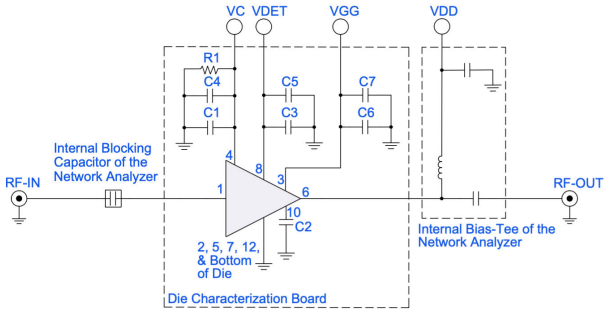

FIGURE 27. MMIC amplifier AVA-054-D+ basic circuit [26].

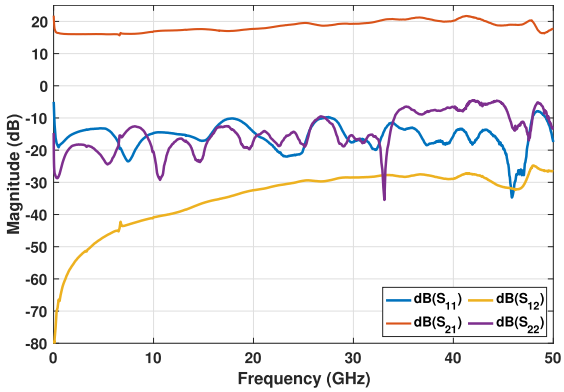

FIGURE 28. S-parameter of MMIC amplifier [26].

is 12 dB. Finally, the yellow curve represents S_{12}, the reverse transmission coefficient. These results indicate that the amplifier maintains a low return loss and provides a consistent gain across the bandwidth, making it effective for wideband applications such as directional coupler, T junction, and microstrip SIW waveguide transition.

IV. CONCLUSION

In this paper, we designed a 4 × 4 directional coupler and several 2-output T-type power dividers, all designed according to the rectangular waveguide standard. In addition, we examined SIW transitions within the same framework. The designs were developed using full-wave electromagnetic simulation software, and the components were subsequently manufactured using SIW technology for validation. The design process started with the rectangular waveguide standard and was subsequently adapted to SIW technology for all devices. These designs were then scaled to an RF-5880 substrate with a dielectric constant of 2.2. After scaling, a soft optimization was performed to enhance the simulation results.

The interior walls of the holes were metalized, which positively contributed to the overall performance of the prototypes. Return loss S_{11} was measured to be less than 20 dB, indicating a 20% bandwidth. These results demonstrated that the devices perform well within the expected operational parameters. However, some experimental results showed discrepancies compared to the simulation results, attributed to the RF-5880 substrate used in the manufactured

prototypes, which caused an average insertion loss of 6 dB in all devices. This aspect is not critical, as the high return loss value (less than 20 dB) and the consistent 20% bandwidth ensure satisfactory device performance.

To address the losses in the conductor walls and the substrate, we propose adding a broadband MMIC amplifier that operates up to the V-band to compensate for these losses. Therefore, in future work, we suggest incorporating an amplifier at the output ports to mitigate these substrate-induced losses.

ACKNOWLEDGMENT

The authors express their gratitude to Complementos Electronicos for their invaluable support during the measurement process.

REFERENCES

[1] K.-J. Tan and X.-Z. Luan, "Compact directional coupler based on substrate integrated waveguide," in *Proc. IEEE Int. Workshop Antenna Technol.*, 2009, pp. 1–4.
[2] C. Tomassoni and M. Bozzi, "Substrate integrated waveguide cavity filters: Miniaturization and new materials for IoT applications," *Radioengineering*, vol. 26, no. 3, pp. 633–641, 2017.
[3] X. Xu, R. G. Bosisio, and K. Wu, "A new six-port junction based on substrate integrated waveguide technology," *IEEE Trans. Microw. Theory Techn.*, vol. 53, no. 7, pp. 2267–2273, Jul. 2005.
[4] K. Wu, D. Deslandes, and Y. Cassivi, "The substrate integrated circuits—A new concept for high-frequency electronics and optoelectronics," in *Proc. Telecommun. Mod. Satell. Cable Broadcast. Serv.*, 2003, pp. 2–9.
[5] M. Bozzi, A. Georgiadis, and K. Wu, "Review of substrate-integrated waveguide circuits and antennas," *IET Microw., Antennas Propag.*, vol. 5, no. 8, pp. 909–920, 2011.
[6] D. Mehdi, N. Keltouma, and F. Mohammed, "Design for tapered transitions from microstrip lines to substrat integrated waveguide at Ka band," *Int. J. Comput. Sci. Issues*, vol. 12, no. 2, pp. 321–326, 2015.
[7] X. Yu, "Analysis and design of radial power combiner on microstrip technology—Análisis y diseño de combinador radial de potencia sobre tecnología microstrip," Master's thesis, Universidad Autónoma de Madrid, Madrid, Spain, 2016.
[8] R. Bouchra and A. Amina, "Development of Ku compact broadband 1×4, 1×8 and 1×16 power dividers with SIW optimized chamfered bends," *Electr. Electron. Eng.*, vol. 9, no. 1, pp. 17–26, 2019.
[9] R. Haro-Báez, J. P. Burbano-Guerrero, and D. S. Benítez, "On the design of truncated T-type power dividers for X-band with SIW technology," in *Proc. IEEE ANDESCON*, 2020, pp. 1–6.
[10] G. Venanzoni, D. Mencarelli, A. Morini, M. Farina, and F. Prudenzano, "Compact substrate integrated waveguide six-port directional coupler for X-band applications," *Radioengineering*, vol. 9, no. 5, p. 1003, 2019.
[11] K. Wu, D. Deslandes, and Y. Cassivi, "The substrate integrated circuits-a new concept for high-frequency electronics and optoelectronics," in *Proc. 6th Int. Conf. Telecommun. Modern Satell., Cable Broadcast. Service (TELSIKS)*, vol. 1, 2003, p. 3.
[12] X.-B. Zhao, F. Wei, P. F. Zhang, and X. W. Shi, "Mixed-mode magic-Ts and their applications on the designs of dual-band balanced out-of-phase filtering power dividers," *IEEE Trans. Microw. Theory Techn.*, vol. 71, no. 9, pp. 3896–3905, Jun. 2023.
[13] X.-B. Zhao, F. Wei, and X. Liu, "Balanced-to-single-ended filtering power divider using multilayer mixed-mode magic-T," *IEEE Trans. Circuits Syst. II, Exp. Briefs*, vol. 70, no. 8, pp. 2859–2863, Jul. 2023.
[14] H. Kumar, R. Jadhav, and S. Ranade, "A review on substrate integrated waveguide and its microstrip interconnect," *J. Electron. Commun. Eng.*, vol. 3, no. 5, pp. 36–40, 2012.
[15] D. Deslandes and K. Wu, "Design consideration and performance analysis of substrate integrated waveguide components," in *Proc. 32nd Eur. Microw. Conf.*, Oct. 2002, pp. 1–4.
[16] J. H. Davis and J. R. Cogdell, "Calibration program for the 16-foot antenna," Elect. Eng. Res. Laboratories, Univ. Texas, Austin, TX, USA, Tech. Rep. NGL-006-69-3, 1987.
[17] D. Deslandes and K. Wu, "Integrated microstrip and rectangular waveguide in planar form," *IEEE Microw. Wireless Compon. Lett.*, vol. 11, no. 2, pp. 68–70, Feb. 2001.
[18] Y. Cassivi, L. Perregrini, P. Arcioni, M. Bressan, K. Wu, and G. Conciauro, "Dispersion characteristics of substrate integrated rectangular waveguide," *IEEE Microw. Wireless Compon. Lett.*, vol. 12, no. 9, pp. 333–335, Sep. 2002.
[19] D. Pozar, *Microwave Engineering*. Hoboken, NJ, USA: Wiley, 2012.
[20] J. A. Ruiz-Cruz, J. R. Montejo-Garai, and J. M. Rebollar, "Short-slot E- and H-plane waveguide couplers with an arbitrary power division ratio," *Int. J. Electron.*, vol. 98, no. 1, pp. 11–24, Jan. 2011.
[21] R. V. Haro-Baez, J. A. Ruiz-Cruz, J. Córcoles, J. R. Montejo-Garai, and J. M. Rebollar, "A new 4 × 4 rectangular waveguide short-slot coupler in 3D printed technology at Ku-band," *Electronics*, vol. 9, no. 4, p. 610, Apr. 2020.
[22] F. Alessandri, M. Giordano, M. Guglielmi, G. Martirano, and F. Vitulli, "A new multiple-tuned six-port riblet-type directional coupler in rectangular waveguide," *IEEE Trans. Microw. Theory Techn.*, vol. 51, no. 5, pp. 1441–1448, May 2003.
[23] A. Suntives, "High-speed data transmission using substrate integrated waveguide-type interconnects," Ph.D. dissertation, Dept. Elect. Comput. Eng., McGill Univ., Montreal, QC, Canada, 2009.
[24] D. Deslandes, "Design equations for tapered microstrip-to-substrate integrated waveguide transitions," in *IEEE MTT-S Int. Microw. Symp. Dig.*, May 2010, pp. 704–707.
[25] Y. Ding and K. Wu, "Substrate integrated waveguide-to-microstrip transition in multilayer substrate," *IEEE Trans. Microw. Theory Techn.*, vol. 55, no. 12, pp. 2839–2844, Dec. 2007.
[26] (2024). *Wideband Amplifier AVA-054-D+*. [Online]. Available: https://www.minicircuits.com/pdfs/AVA-054-D

RAÚL HARO-BÁEZ (Senior Member, IEEE) received the B.Eng. degree in electronic and telecommunications engineering and the M.Gs. degree in information networks and connectivity from Escuela Politécnica del Ejército, Quito, Ecuador, in 2002 and 2012, respectively, and the M.Sc. degree in investigation and innovation in TICs and the Ph.D. degree in computing and telecommunication from Escuela Politécnica Superior (Universidad Autónoma de Madrid), Madrid, Spain, in 2013 and 2023, respectively. In 2003, he joined Universidad de las Fuerzas Armadas—ESPE, Sangolqui, Ecuador, where he has been an Associate Professor, since 2003, and a Full Professor, since 2005. His research interests include power distribution networks, communications systems, antennas, array antennas, and passive and active devices.

HENRY CARVAJAL MORA (Senior Member, IEEE) received the B.Sc. degree (Hons.) in electronics and telecommunications engineering from Armed Forces University—ESPE, Ecuador, in 2009, and the M.Sc. and Ph.D. degrees in electrical engineering from the School of Electrical and Computer Engineering (FEEC), University of Campinas (UNICAMP), Brazil, in 2014 and 2018, respectively. He was the Director of the Technology Transfer Area in the Education, Science and Technology Secretariat (SENESCYT), Ecuador, in 2018. He obtained the HCIA-5G Certification from Huawei, in 2020. He is currently an Assistant Professor with Universidad de Las Américas (UDLA), Ecuador. His research interests include fading channels, diversity-combining systems, orthogonal and non-orthogonal multiple access, multiuser detection, MIMO, physical-layer security, 5G, and B5G technologies.

NATHALY OROZCO GARZÓN (Senior Member, IEEE) received the degree in electronic and telecommunications engineering from Armed Forces University—ESPE, Ecuador, in 2011, and the M.Sc. and Ph.D. degrees in electrical engineering from the University of Campinas (UNICAMP), Brazil, in 2014 and 2018, respectively. She obtained the HCIA-5G Certification from Huawei, in 2020. She is currently an Assistant Professor with Universidad de Las Américas (UDLA), Quito, Ecuador. Her research interests include digital communications, with a specific emphasis on orthogonal and non-orthogonal multiple access, fading channels, MIMO, cognitive systems, opportunistic transmissions, and 5G technologies.

KATHERINE HERRERA received the B.Sc. degree in electronics and telecommunication engineering from Armed Forces University—ESPE, Sangolquí, Ecuador, in 2019, and the Master of Business Administration degree in big data and design thinking from the EAE Business School, Spain, in 2021. She obtained the Fortinet Certified Associate Cybersecurity certification from Fortinet, JNCIS-SP from Juniper, and NCP-MCI from Nutanix. She was a Security and Communication Project Manager with the Ministry of Justice in Spain. She is currently a Development Engineer at the company Indra Solutions TI S.L.

DIEGO BENÍTEZ (Senior Member, IEEE) received the B.Eng. degree in electrical engineering from Escuela Politécnica Nacional, Quito, Ecuador, in 1994, and the M.Sc. and Ph.D. degrees in electrical engineering from the Institute of Science and Technology, The University of Manchester, Manchester, U.K., in 1997 and 2001, respectively. From 2005 to 2007, he was a Postdoctoral Research Associate with the Sensing, Imaging, and Signal Processing Research Group, School of Electrical and Electronic Engineering, The University of Manchester. From 2007 to 2012, he was a Senior Research Engineer with the Bosch Research and Technology Center, Pittsburgh, PA, USA, where he was also an Academic Visitor with the Institute for Complex Engineered Systems and the INFER Laboratory, Carnegie Mellon University. From 2012 to 2014, he was a Visiting Research Scholar with Universidad de las Fuerzas Armadas ESPE under the ''Prometeo Program'' of SENESCYT, Ecuador. He is currently a full-time Professor with Universidad San Francisco de Quito (USFQ), Quito, where he co-founded and led the Applied Signal Processing and Machine Learning Research Group. He holds 26 granted and pending U.S. and overseas patents. His research interests include signal and image processing, pattern recognition and machine learning, intelligent instrumentation and measurement systems for medical, energy management, security, and smart building applications. He has authored more than 160 refereed journals and conference papers on these topics. He has served as the IEEE Ecuador Section Chair, from 2018 to 2019.